ACS APPLIED MATERIALS & INTERFACES

Research Article

www.acsami.org

Hierarchical Nanoporous Silica Films for Wear Resistant Antireflection Coatings

Norihiro Mizoshita,* Masahiko Ishii, Naohiko Kato, and Hiromitsu Tanaka*

Toyota Central R&D Laboratories, Inc., Nagakute, Aichi 480-1192, Japan

Supporting Information

ABSTRACT: High-performance antireflection (AR) layers were prepared by depositing hierarchical nanoporous silica films on glass substrates. We designed a composite layer consisting of mesoporous silica nanoparticles (MSNs) and a mesoporous silica matrix. The introduction of bimodal nanoporous structures, i.e., independent nanopore formation within the MSN and within the matrix, was achieved by using surface-protected MSNs and a polymeric nonionic surfactant template during the fabrication process. A porosity of more than 40% was achieved for composite AR materials. The protrusion of MSNs from the matrix led to spontaneous formation of nanoscale roughness on the surface of the coatings, which enhanced the AR properties. The solid bonding of the MSNs to the nanoporous matrices played an important role in the achievement of high mechanical durability. The optimal nanoporous coating, which contained ca. 50 wt % MSN, exhibited high transparency (91.5−97.5%) and low reflectance (<2.2%), over the whole range of visible light wavelengths, and sufficient wear resistance.

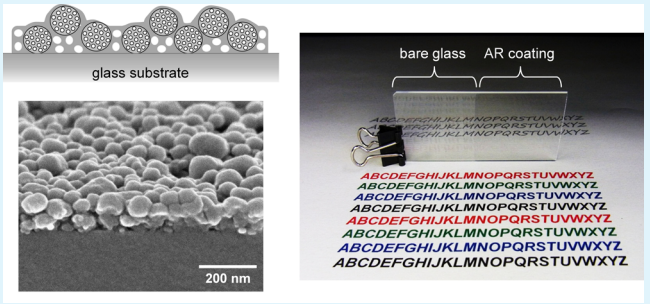

KEYWORDS: *antireflection, calcination, mesoporous silica, nanoparticles, self-assembly*

INTRODUCTION

The fabrication of antireflection (AR) coatings on substrate surfaces is of great importance in many optical applications.[1,2] Suppression of the reflection of light at the surface or interface of transparent substrates leads to improved optical properties (transparency and visibility) of windows, lenses, displays, photodetectors, etc. Recently, the enhancement of solar cell performance by AR coatings has also attracted much attention.[3,4]

The reflectance (R) at an interface formed by media with refractive indices of n_1 and n_2 is given by $R = (n_1 - n_2)^2/(n_1 + n_2)^2$ at normal incidence. For example, the interface of air (n_1 = 1.0) and a glass substrate (n_2 = 1.5) gives an R of ∼4%; therefore, the total reflectance of a glass substrate in air becomes ∼8%, owing to the reflection on both sides of the substrate. AR coatings are designed to suppress the reflection of light from the air−coating and coating−substrate interfaces, on the basis of thin film interference.[1,2] A single-layer coating exhibiting the minimum reflection satisfies the following conditions: (i) the thickness of the coating layer should be $\lambda/4n_c$, where λ is the incident wavelength and n_c is the refractive index of the coating; (ii) $n_c = (n_1n_2)^{1/2}$. Fundamental AR coatings consist of vacuum-deposited dielectric materials (e.g., magnesium fluoride with a refractive index of 1.38). However, in order to achieve high optical performance such as broad-band AR properties over oblique incident angles, complex multilayer coatings need to be fabricated, which is too costly and not suitable for mass production. Low values of n_c close to $(n_1n_2)^{1/2}$ (e.g., n_c = 1.22 for n_1 = 1.0 and n_2 = 1.5) are also necessary for decreasing the reflectance.

One useful method to fabricate low-refractive-index (low-n) materials is the introduction of nanoporous structures. Mesoporous silica films synthesized by surfactant-directed polycondensation of alkoxysilane precursors have been widely studied as low-n coating materials.[5−7] Microporous silica and mesoporous organosilica films are also candidates for low-n materials.[8,9] On the other hand, aggregated nanoparticles with interparticle voids have been used to increase porosity of AR coatings.[10−12] Not only nonporous nanoparticles but also mesoporous silica nanoparticles (MSNs) are useful as components of low-n materials.[13−15] Recently, chemical modification and mass production of MSNs have been achieved,[16−18] which increases the applicability of MSNs as a practical low-n component. Porous polymers have also been proposed as AR coatings.[2] These studies have revealed that materials with extremely high porosity can exhibit very low refractive indices of less than 1.2.

The formation of subwavelength-scale nanostructures on substrate surfaces, represented by the so-called "moth-eye" structure, is another effective way of inducing low reflectance and broad-band AR properties.[1,2,19] Such nanostructured surfaces behave like a graded-refractive-index AR layer. AR coatings with nanoscale projections, fibers, rods, or reliefs, have

Received: June 25, 2015
Accepted: August 14, 2015
Published: August 14, 2015

DOI: 10.1021/acsami.5b05659
ACS Appl. Mater. Interfaces 2015, 7, 19424−19430

been fabricated through a variety of methods, such as chemical vapor deposition, plasma etching, and nanoimprint lithography.[20−25]

However, these low-*n* and AR coating materials, which exhibit extremely high porosity and/or consist of nano-objects with high aspect ratios, often lack the mechanical durability needed for practical use. Although AR coatings based on porous nanoparticles can be stabilized by filling the interparticle voids with a matrix, the use of nonporous matrix greatly degrades optical properties. It is necessary to establish a new material design approach for nanostructured AR coatings that will allow them to be fabricated by a simple process and to exhibit both useful optical properties and sufficient mechanical durability. In practical applications as glass windows, the decrease in the reflectance is effective for improving visibility; therefore, it is important to decrease reflectance desirably to less than 2%, securing adequate transparency in the visible light wavelength region.

Here, we report the facile preparation of a new type of antireflective mesoporous coatings with wear resistance toward application in indoor glass windows. Figure 1 shows the

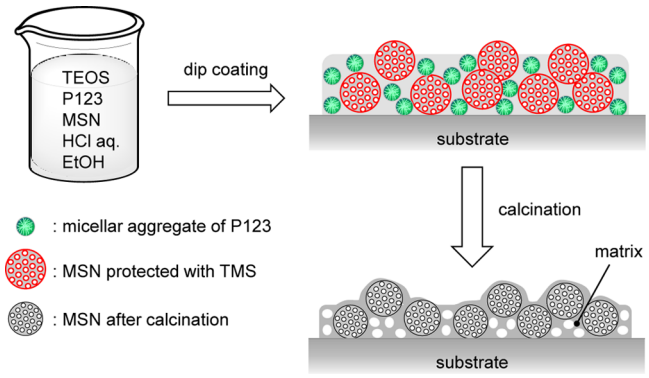

Figure 1. Fabrication of antireflection films consisting of MSNs and a mesoporous silica matrix.

fabrication process of the nanoporous silica coatings, which is based on the dip-coating method. We designed hierarchically nanoporous thin films (MesoMSN) that consisted of MSNs and a mesoporous silica matrix and possessed nanoscale surface roughness. The mesoporous matrix filling the interparticle voids between MSNs was expected to enhance the mechanical durability of the coating. We assumed that a low surface roughness (e.g., < 100 nm) with low aspect ratios would guarantee wear resistance of the coatings. It was confirmed by simulations that a surface roughness of even ±40 nm had a satisfactory effect on reducing the reflection of light (see Supporting Information, Figure S1). In order to induce spontaneous nanoroughness formation and introduce nanoporous structures into both the matrix and the nanoparticles, the following design concepts were incorporated into the present fabrication process: (i) when the film matrix and MSNs were mixed in appropriate ratios, the MSNs protruded from the film surface, leading to spontaneous formation of a nanorough surface; (ii) as a template to form mesopores in matrices, we used the polymeric nonionic surfactant P123, whose micellar aggregates are larger than the nanopore size (3.5 nm) of the MSNs, enabling the nanopores within the matrices and MSNs to form independently; (iii) the surface of the MSNs was protected with trimethylsilyl (TMS) groups to prevent tetraethoxysilane (TEOS), a matrix material, from reacting with the MSNs in the precursor mixtures and during the dip-coating process; (iv) on calcination of the dip-coated films, the protective TMS groups of the MSNs as well as the P123 template decompose, which should result in covalent bond formation between the matrix and the MSNs and enhance the mechanical durability of the coatings. In the present study, high-performance nanoporous silica coatings exhibiting high transparency, AR properties, and wear resistance were successfully obtained by single coating of precursor dispersions with appropriate matrix/MSN ratios.

EXPERIMENTAL SECTION

General Methods. Nitrogen adsorption−desorption isotherms were measured using a Quantachrome Autosorb-1 sorptometer at −196 °C. Prior to measurements, all samples were outgassed at 110 °C for 2 h. Pore size distributions were determined using the density functional theory (DFT) method (the DFT kernel used: N_2 at 77 K on silica, cylindrical pore, NLDFT equilibrium model). Pore volumes were estimated by the *t*-plot method. ^{29}Si magic-angle spinning (MAS) NMR spectra were recorded on a Bruker Avance 400 spectrometer (at 79.49 MHz) using 7 mm zirconia rotors and a sample spinning frequency of 4 kHz. The chemical shifts for all spectra were referenced to tetramethylsilane at 0 ppm. Scanning electron microscopy (SEM) was conducted on a Hitachi S-4300 with an acceleration voltage of 2.0 kV. Transmission electron microscopy (TEM) was performed on a Jeol JEM-2010FEF with an acceleration voltage of 200 kV. Atomic force microscope (AFM) observation was performed using a NanoNavi E-sweep scanning probe microscope system (Hitachi) with a cantilever SI-DF20. X-ray diffraction measurements were performed on a Rigaku RINT-TTR diffractometer with Cu−Kα radiation (50 kV, 300 mA). The particle size distribution of MSNs was determined in ethanol by the dynamic light scattering method using a Nikkiso UPA250EX. Transmission spectra were recorded using a Jasco V-670 spectrometer. The measuring area is ca. 1.1 cm^2. The reflectance was measured using a Soma S-2650 system. The measuring area is ca. 0.8 cm^2. In this measurement system, the reflectance measured for wavelength less than 500 nm has an error of ca. ± 1% due to the characteristics of the apparatus. The refractive index was measured using an M-2000U spectroscopic ellipsometer (J.A. Woollam Co., Inc.). The data were taken at incident angles of 55, 60, and 65°. A regression of the data was performed using the Cauchy dispersion law.

Materials. All reagents and solvents were purchased from Aldrich and Tokyo Chemical Industry and used without further purification. As a template surfactant for matrices, the nonionic surfactant P123 (Aldrich, $HO(CH_2CH_2O)_{20}(CH_2CH(CH_3)O)_{70}(CH_2CH_2O)_{20}H$) was used. TMS-protected MSN was prepared using cetyltrimethylammonium bromide as a template surfactant according to the method reported by Okubo et al.[13] The average particle size, as determined by dynamic light scattering measurements, was ca. 100 nm, and the average pore size was calculated to be 3.5 nm from the nitrogen adsorption−desorption isotherm by using the DFT method (see Supporting Information, Figure S2).

Preparation of MesoMSN-35. TMS-protected MSN was dispersed in ethanol at a concentration of 2.0 wt %. To this dispersion (6.0 mL), TEOS (0.64 g), P123 (0.16 g), 2 M hydrochloric acid (80 μL), and water (80 μL) were added to adjust the MSN fraction to be ca. 35 wt % in the final nanoporous silica film. The precursor dispersion was stirred at 25 °C for 24 h. A borosilicate glass slide (S1112, Matsunami Glass Ind., Ltd.) was dip-coated (25 × 25 mm) with the precursor dispersion at a liftoff rate of 20 mm/min. After drying at 25 °C for 24 h, the dip-coated film was calcined at 500 °C for 4 h, yielding a glass substrate coated with MesoMSN-35 on both sides.

Preparation of MesoMSN-50. MesoMSN-50 was prepared by a procedure similar to that used for MesoMSN-35, using a 3.5 wt % dispersion of TMS-protected MSN in ethanol (6 mL), TEOS (0.56 g), P123 (0.14 g), 2 M hydrochloric acid (80 μL), and water (80 μL). The

DOI: 10.1021/acsami.5b05659
ACS Appl. Mater. Interfaces 2015, 7, 19424−19430

MSN fraction was adjusted to be ca. 50 wt % in the final nanoporous silica film.

Preparation of MesoMSN-65. MesoMSN-65 was prepared by a procedure similar to that used for MesoMSN-35, using a 5.0 wt % dispersion of TMS-protected MSN in ethanol (6 mL), TEOS (0.48 g), P123 (0.12 g), 2 M hydrochloric acid (80 μL), and water (80 μL). The MSN fraction was adjusted to be ca. 65 wt % in the final nanoporous silica film.

Preparation of Meso-F. A mesoporous film (Meso-F) containing no MSN was prepared using P123 and TEOS. A mixture of ethanol (15 mL), TEOS (2.0 g), P123 (0.50 g), 2 M hydrochloric acid (200 μL), and water (200 μL) was stirred at 25 °C for 24 h. A glass substrate was dip-coated with the precursor dispersion at a liftoff rate of 20 mm/min. After drying at 25 °C for 24 h, the dip-coated film was calcined at 500 °C for 4 h, yielding a glass substrate coated with Meso-F.

Wear Resistance and Hardness Test. Wear resistance test was performed by rubbing the surface of the coatings with cotton wool at a high pressure of 5 kg/cm^2. After rubbing the coating 50 times, the surface was observed using an optical microscope. Hardness was evaluated by the pencil hardness test method based on JIS K5600-5-4 (Japanese Industrial Standards) with pencils (Mitsubishi Co.) having hardness ranging from 6B (the softest) to 6H (the hardest). The coatings were scratched with the flat end of the pencil placed at a 45° angle to the surface with a loading of 750 g. The existence of the scratch was evaluated using an optical microscope. For the MesoMSN coating with nanoscale roughness, the pencil lead remaining on the surface was removed by plastic erasers before visual observation.

RESULTS AND DISCUSSION

Structures of Mesoporous Coatings. MesoMSN-*m* coatings with different matrix/MSN ratios (*m*: approximate wt % of MSN) were prepared by dip-coating of glass substrates with precursor dispersions and subsequent calcination treatment (Figure 1). MesoMSN-35 and MesoMSN-50 were obtained as transparent films, whereas MesoMSN-65 exhibited a slightly opaque appearance. Figure 2 shows the SEM images of the coatings before and after calcination. Thin coatings (100−200 nm) were formed on the surface of the glass substrates. For MesoMSN-35, most of the MSNs were embedded within the matrix film (Figure 2a). After calcination, the film thickness decreased from ca. 180 to 100 nm, and the surface morphology became almost flat (Figure 2b). In contrast, MesoMSN-50 had a rough surface with protruding MSNs. The film thickness is ca. 140 nm after calcination. The height of individual protrusions was 20−100 nm. The distribution of refractive index in the direction of film thickness is expected to be caused by the rough surface structures though their effect might be smaller than those of conventional moth-eye films or multilayered coatings. The MSNs were well bonded to the matrix as seen in Figures 2c and 2d. In this coating, the formation of a surface roughness by the protrusion of the MSNs seems to be counterbalanced with the bonding of the MSNs due to the appropriate matrix/MSN ratio. MesoMSN-65, which contained a higher amount of MSN, also exhibited the formation of a surface roughness and the bonding of MSNs to the matrix (Figures 2e and 2f). The film thickness is ca. 180 nm after calcination. However, there were many cracks in the coating (Figure 2f). The slightly opaque appearance of the MesoMSN-65 was presumably due to light scattering caused by microscale heterogeneous structures. The agglomeration of MSNs during dip-coating and calcination could not be suppressed because of the matrix deficiency in MesoMSN-65. The surface roughness was evaluated by calculating arithmetic average of absolute values (R_a; see

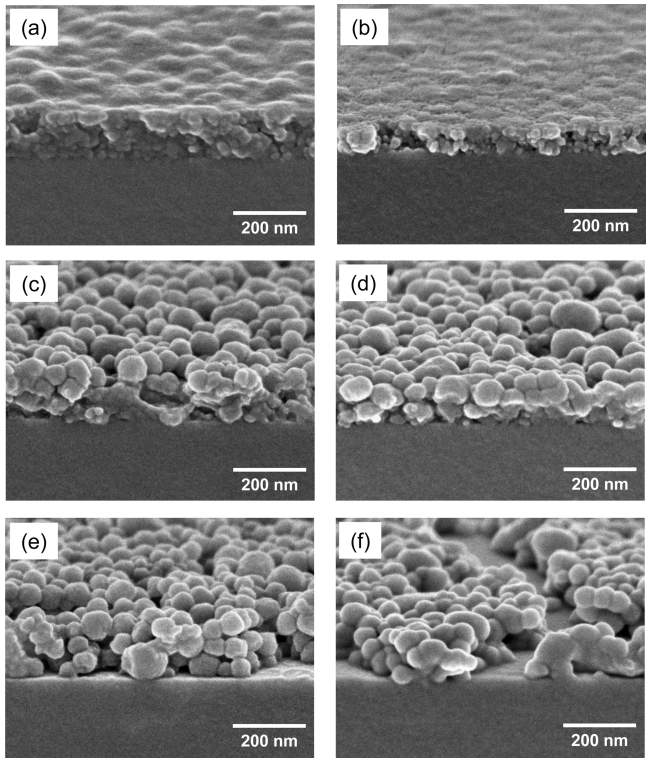

Figure 2. SEM images of mesoporous silica coatings before (a, c, e) and after calcination (b, d, f): (a, b) MesoMSN-35; (c, d) MesoMSN-50; (e, f) MesoMSN-65.

Supporting Information, Figure S5) from AFM topographic images. The value of R_a was 2.2 nm for MesoMSN-35, whereas it was 16.0 nm for MesoMSN-50. Although it was difficult to average the roughness of the MesoMSN-65 because of the large cracks, the R_a calculated for the crack-free region was 13.0 nm. These values are probably underestimated because the AFM probes cannot enter interparticle voids deeply and the AFM images were constructed by the integration of surface contours. The relatively large R_a of MesoMSN-50 also indicates the spontaneous formation of nanorough surface by the protrusion of MSNs.

The changes in the chemical structure of the silica framework and of the surface of MSNs that occurred upon calcination were examined by comparing the ^{29}Si MAS NMR spectra of calcined MesoMSN-50 with those of noncalcined TMS-protected MSNs (Figure 3a). Three main peaks are observed in the case of noncalcined MSNs. The peaks at −100.6 and −109.4 ppm correspond to the Q^3 and Q^4 species (Q^n: $Si(OSi)_n(OH)_{4-n}$) of the silica framework, respectively. The peak at 13.5 ppm is attributed to the M^1 species corresponding to the surface protection group TMS ($(SiO)Si(CH_3)_3$). Upon calcination of the matrix/MSN composite film, the M^1 species disappeared completely, leaving behind mainly the Q^4 species. These results demonstrate the calcination-induced TMS decomposition and siloxane network rearrangement, suggesting covalent bond formation between the matrix and MSNs (Figure 3b).

The porosity of the MesoMSN-50 film was determined by nitrogen adsorption−desorption isotherm measurements. Figure 4 plots pore size distributions and nitrogen adsorption−desorption isotherms of a calcined matrix film (Meso-F, containing no MSNs), MSNs, and MesoMSN-50. The Meso-F

DOI: 10.1021/acsami.5b05659
ACS Appl. Mater. Interfaces 2015, 7, 19424−19430

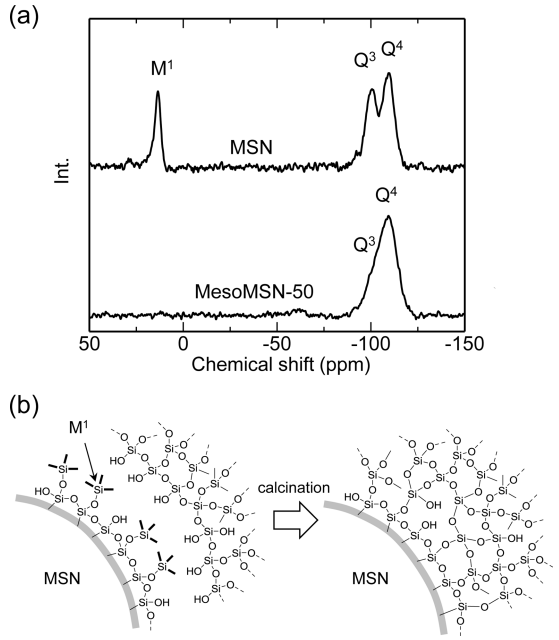

Figure 3. (a) Solid-state ^{29}Si MAS NMR spectra of TMS-protected MSN and calcined MesoMSN-50; (b) schematic illustration of siloxane bond formation by calcination.

exhibited a type-IV isotherm, typical of mesoporous materials. The pore diameter was ca. 4.0 nm (Figure 4a). The calcined MSNs had nanopores with a diameter of 2.6 nm (Figure 4b), which is 0.9 nm smaller than that of noncalcined MSNs (3.5 nm). The pore size distribution of MSNs also showed a broad peak around 15 nm. This is attributable to interparticle porosity of the spherical MSNs. On the other hand, the nitrogen isotherm of MesoMSN-50 indicated the formation of two sizes of nanopores with diameters of 2.0−2.4 and 5.0 nm, respectively (Figure 4c). The smaller nanopores are those inside the MSNs, whereas the larger are those formed within the matrix. It should be noted that the large nanopores (~15 nm) observed for calcined MSN were under the detection limit for MesoMSN-50. This suggests that the interparticle voids between the MSNs were effectively filled with the nanoporous silica matrix. The pore volume of MesoMSN-50 was calculated to be 0.34 cm^3/g. The porosity of MesoMSN-50 is 43%, if the density of silica is assumed to be 2.2 g/cm^3. The porosities of calcined Meso-F and MSNs attributed to surfactant-templated nanopores are calculated to be 40 and 43%, respectively. These results also support the bimodal nanopore formation in MesoMSN-50.

XRD measurements of the mesoporous materials revealed the arrangement of the nanopores formed in MesoMSN composite coatings. Figure 5 shows XRD patterns of Meso-F, MSNs, and MesoMSN-50. The Meso-F and MSNs exhibited XRD peaks at d = 7.1 and 3.3 nm, respectively, indicating the formation of periodic nanopores. In contrast, only one peak at d = 3.4 nm was observed for MesoMSN-50. This peak was attributed to the periodicity of nanopores within the MSNs. These results indicated that the 5.0 nm nanopores formed in the matrix of MesoMSN-50 had no periodic arrangement. It is not surprising that the matrix that infiltrated into the narrow interparticle voids between the MSNs did not exhibit periodically arranged nanopores.

The formation of bimodal nanoporous structures in the MesoMSN-50 coating was directly verified by TEM observation

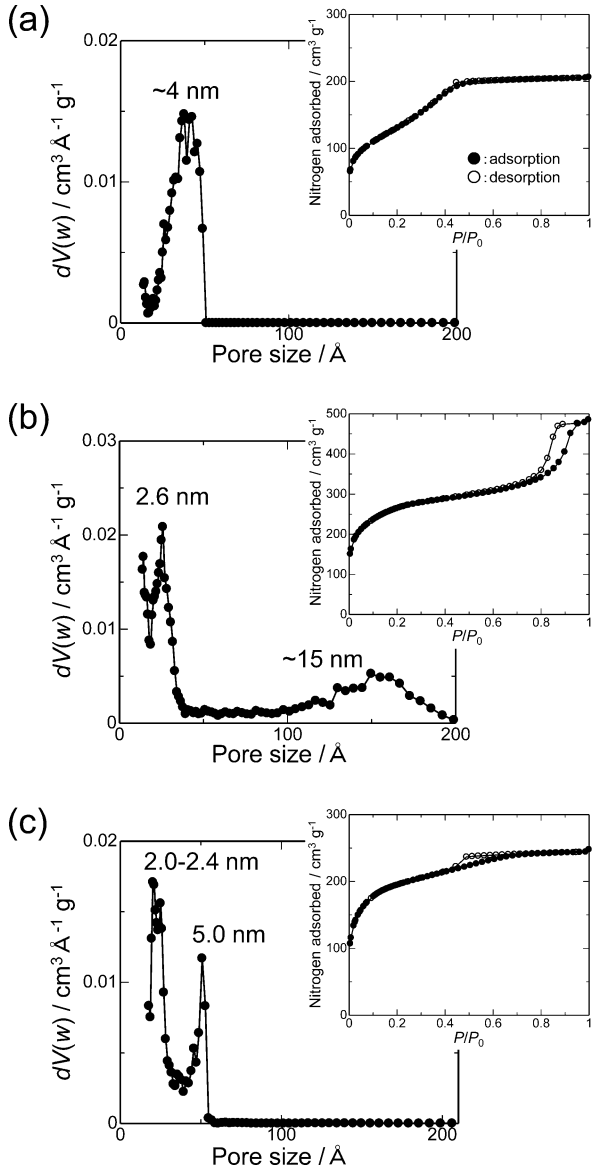

Figure 4. Pore size distribution of (a) Meso-F, (b) MSN, and (c) MesoMSN-50 after calcination. Inset: nitrogen adsorption−desorption isotherms.

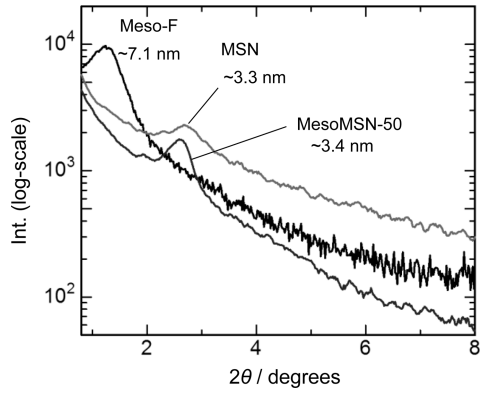

Figure 5. XRD patterns of Meso-F, MSN, and MesoMSN-50 after calcination.

(Figure 6). A striped structure with a periodicity of ca. 3 nm is observed for globular regions corresponding to MSNs. On the

DOI: 10.1021/acsami.5b05659
ACS Appl. Mater. Interfaces 2015, 7, 19424−19430

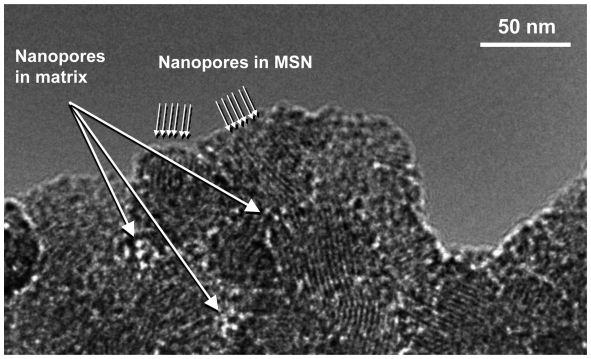

Figure 6. TEM image of MesoMSN-50.

other hand, 5.0 nm nanopores can be seen in the narrow regions between the MSNs, corresponding to the matrix. The TEM image also shows that the MSNs are well bonded to the nanoporous matrix.

Optical and Mechanical Properties. MesoMSN-50 exhibited significant optical properties. Figure 7 shows the

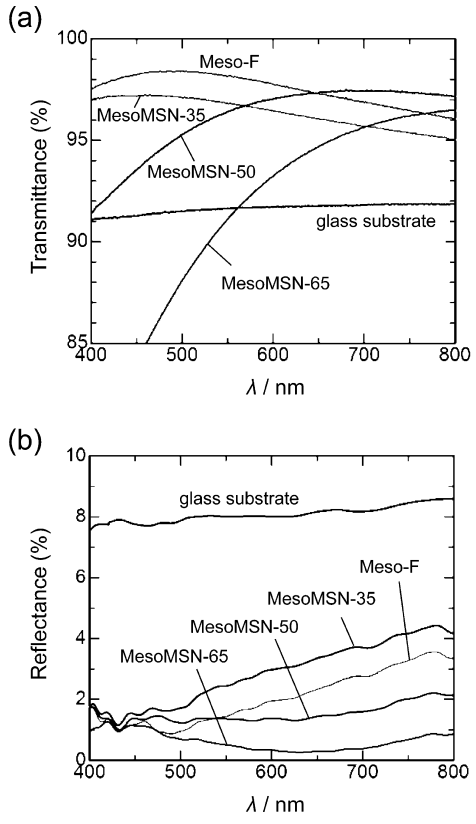

Figure 7. Optical properties of mesoporous silica coated glass substrates: (a) transmittance; (b) reflectance.

transmittance and reflectance of the MesoMSN-*m*-coated glass substrates. The optical properties of bare and Meso-F-coated glass substrates are also shown for comparison. Nanoporous coatings containing 50 wt % or less MSN showed a higher transmittance than the bare glass substrate over the whole range of visible-light wavelengths (Figure 7a). AR behavior was observed for all substrates coated with mesoporous materials (Figure 7b). The decreases in the reflectance for the MesoMSN films are more significant than those reported for MSN-based films stabilized by a nonporous silica matrix,[13] indicating the effectiveness of the introduction of mesopores within the matrix. MesoMSN-50 and MesoMSN-65 exhibited excellent broad-band AR properties. In contrast, the AR behavior of the MesoMSN-35-coated substrate, whose surface was almost flat (Figure 2b), was comparable or slightly inferior to Meso-F. These results suggest that the surface roughness formed by the protrusion of nanoparticles contributes significantly to the improvement in AR properties. As a result, MesoMSN-50 exhibited both high transparency and fine AR behavior. The maximum transmittance observed for MesoMSN-50 was 97.5% at 680 nm. The reflectance of MesoMSN-50 was 1.1−2.2% (ca. 0.6−1.1% for one side) in the visible light wavelength range. The photograph in Figure 8 demonstrates the AR properties of

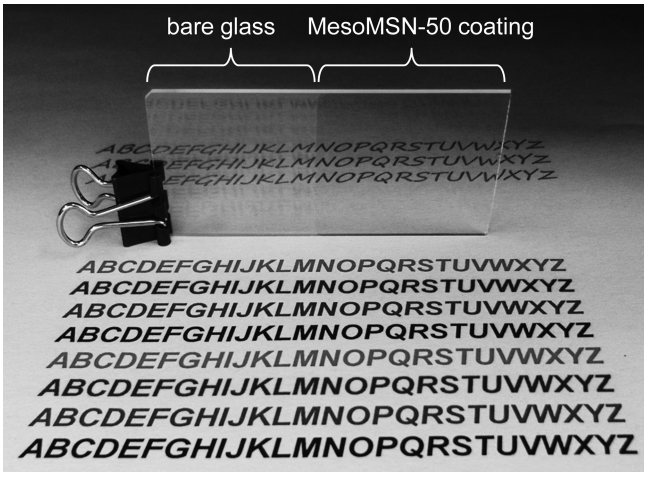

Figure 8. Photograph of a glass substrate coated with MesoMSN-50.

MesoMSN-50; the printed letters are reflected on the bare glass substrate, whereas light reflection is strongly suppressed on the MesoMSN-50-coated surface. The photograph also indicates the high transparency of the MesoMSN-50 coating.

The average refractive indices of the MesoMSN-*m* coatings were estimated by spectroscopic ellipsometry. Figure 9 plots the refractive indices of the nanoporous coatings as a function of wavelength. The MesoMSN-*m* coatings exhibited apparent refractive indices of around 1.3, and the values tended to

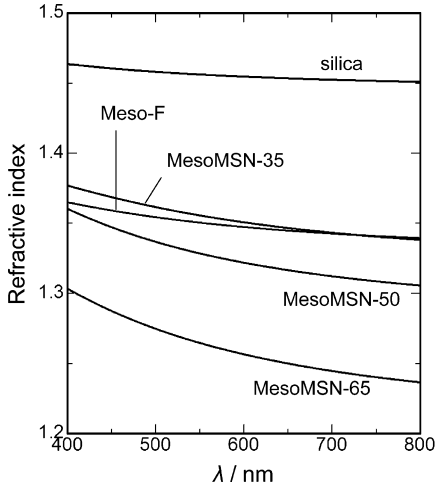

Figure 9. Refractive indices of mesoporous coatings, calculated on the basis of the Cauchy model, as a function of wavelength.

DOI: 10.1021/acsami.5b05659
ACS Appl. Mater. Interfaces 2015, 7, 19424−19430

decrease with increasing amount of MSN. For example, the refractive indices of MesoMSN-35, MesoMSN-50, and MesoMSN-65 were 1.35, 1.32, and 1.26, respectively, at λ = 600 nm. These values fall between 1.00 (air) and 1.51 (glass substrate), which is desirable for inducing AR properties. However, it should be noted that the results were obtained through a curve fit based on the Cauchy model, i.e., the coatings were treated as homogeneous materials. The present refractive index values are presumably governed more by morphological features (voids, roughness, and cracks) of the MesoMSN coatings (Figure 2), than by the refractive index of the coating material itself. It should also be noted that the values of refractive index are higher than those expected from the porosity of the coatings. The increase in the refractive index is probably due to the adsorption of water in air onto the hydrophilic surface of MesoMSN films.[12]

For application to transparent substrates, the optical loss (= 100 − (transmittance + reflectance) [%]) induced by coating materials based on nanoparticles should be discussed. For Meso-F, which contains no MSN, and for MesoMSN-35, which exhibits no distinct spherical features on its surface, the optical losses are negligible (<0.5% for one side). The optical loss for MesoMSN-50 is also less than 1% for one side at wavelengths longer than 600 nm. However, a decrease in light transmittance is clearly observed in the short wavelength region. This behavior is associated with the Rayleigh scattering of nanoparticles. It is known that the Rayleigh cross-section is valid for spherical particles with sufficiently small radii compared to the wavelength of scattered light.[26,27] Since we used MSNs with an average diameter of ca. 100 nm, the sub-wavelength-scale structures formed by the MSNs contribute to the induced Rayleigh scattering. If the decrease in the transmittance due to the light scattering is suppressed by the more precise design of the composite structures, significant AR coatings with higher transparency will be obtained. Improving overall optical properties through size and morphology control of particulate structures is an important challenge in the development of MSN-based optical coatings.

Finally, the wear resistances of the MesoMSN-*m* coatings were measured to assess their suitability for practical use. The MesoMSN-*m* coatings were rubbed 50 times with cotton wool at a high pressure of 5 kg/cm^2. The results of wear resistance tests are tabulated with representative optical properties in Table 1. The MesoMSN-*m* coatings containing 50 wt % or less MSNs exhibited high wear resistance. For these coatings, neither scratches nor peeling was observed after the wear resistance test. The solid bonding of MSNs to the matrix and the formation of siloxane bonds between them contribute to the high mechanical durability. The surface roughness with low aspect ratios formed by the protrusion of spherical MSNs is thought to ensure wear resistance. On the other hand, the MesoMSN-65 coating partly peeled off the substrate. The formation of cracks in the coating (Figure 2f) presumably degrades the mechanical durability. As reference samples, thin films prepared using MSNs (80 wt %) and a small amount of silica binder (poly(dimethoxysiloxane) (PDMS), 20 wt %) were also subjected to wear resistance testing. These MSN/PDMS coatings showed a high transmittance of over 95% and a low reflectance of less than 2.0% at 600 nm, owing to the high porosity resulting from mesopores and interparticle voids. However, they had no wear resistance regardless of the calcination treatment (Table 1). We also evaluated the hardness of the mesoporous coatings with a conventional pencil hardness test.[28] The mesoporous coatings durable for the harsh rubbing test with cotton wool exhibited 3H or higher hardness. The hardness is similar to that of a hard coating (no scratch until 2H) used in flat panel displays or touch panels.[28] A MesoMSN-65 film having cracks showed a variation in the data. The hardness of the reference coatings (MSN/PDMS) having interparticle voids was 2B even after calcination. The increase in the fraction of MSN leads to a decrease in the hardness, probably due to the promotion of the formation of structural voids and roughness. These results suggest that the formation of hierarchically nanostructured films with appropriate MSN-to-matrix ratios is essential to achieve adequate optical properties and high mechanical durability.

Table 1. Optical Properties (at λ = 600 nm) and Wear Resistance of the Mesoporous Silica Coatings

Coatings	Transmittance (%)	Reflectance (%)	Wear resistance test[a]	Pencil hardness
bare glass	91.7	7.9		
Meso-F	97.8	1.9	No damage	4H−5H
MesoMSN-35	96.2	3.0	No damage	4H
MesoMSN-50	97.0	1.4	No damage	3H
MesoMSN-65	93.2	0.3	Partly peeled	F−2H
MSN/PDMS (8/2, w/w)[b]	95.2	0.9	Completely peeled	<6B
MSN/PDMS (8/2, w/w)[c]	96.2	1.8	Completely peeled	2B

[a]Surface rubbing with cotton wool at 5 kg/cm^2. [b]Spin-coated film prepared from a dispersion of MSNs in ethanol containing a catalytic amount of HCl and poly(dimethoxysiloxane) (PDMS) as a binder. [c]After calcination at 500 °C for 4 h.

CONCLUSION

A new type of AR coating with wear resistance was developed using hierarchically nanoporous silica thin films made of MSNs and a mesoporous silica matrix. The nanoporous structures and nanoscale surface roughness were found to enhance optical properties significantly. The solid bonding of the MSNs to mesoporous silica matrices imparted the coating with wear resistance. It should be noted that the present nanostructured films can be prepared with a simple coating process that requires no complicated steps such as lamination, chemical vapor deposition, or etching treatment. This is a great advantage in terms of low-cost fabrication and mass production. It was also found that the present MesoMSN coatings exhibited antifogging properties owing to their high hydrophilicity and large surface area, which will be further examined in the near future. Functional AR coatings are expected to improve with increasing productivity and structural controllability of mesoporous nanoparticles.

ASSOCIATED CONTENT

Supporting Information

The Supporting Information is available free of charge on the ACS Publications website at DOI: 10.1021/acsami.5b05659.

Simulation of reflectance, structural properties of MSN, and supplementary SEM and TEM images (PDF)

AUTHOR INFORMATION

Corresponding Authors

*E-mail: nmizoshita@mosk.tytlabs.co.jp.

DOI: 10.1021/acsami.5b05659
ACS Appl. Mater. Interfaces 2015, 7, 19424−19430

*E-mail: e0884@mosk.tytlabs.co.jp.

Notes

The authors declare no competing financial interest.

■ ACKNOWLEDGMENTS

The authors thank Mr. H. Kadoura for performing SEM observations.

■ REFERENCES

(1) Raut, H. K.; Ganesh, V. A.; Nair, A. S.; Ramakrishna, S. Anti-Reflective Coatings: A Critical, In-Depth Review. *Energy Environ. Sci.* **2011**, *4*, 3779−3804.
(2) Li, X.; Yu, X.; Han, Y. Polymer Thin Films for Antireflection Coatings. *J. Mater. Chem. C* **2013**, *1*, 2266−2285.
(3) Lee, Y.-J.; Ruby, D. S.; Peters, D. W.; McKenzie, B. B.; Hsu, J. W. P. ZnO Nanostructures as Efficient Antireflection Layers in Solar Cells. *Nano Lett.* **2008**, *8*, 1501−1505.
(4) Tao, M.; Zhou, W.; Yang, H.; Chen, L. Surface Texturing by Solution Deposition for Omnidirectional Antireflection. *Appl. Phys. Lett.* **2007**, *91*, 081118.
(5) Falcaro, P.; Grosso, D.; Amenitsch, H.; Innocenzi, P. Silica Orthorhombic Mesostructured Films with Low Refractive Index and High Thermal Stability. *J. Phys. Chem. B* **2004**, *108*, 10942−10948.
(6) Falcaro, P.; Malfatti, L.; Kidchob, T.; Giannini, G.; Falqui, A.; Casula, M. F.; Amenitsch, H.; Marmiroli, B.; Grenci, G.; Innocenzi, P. Hierarchical Porous Silica Films with Ultralow Refractive Index. *Chem. Mater.* **2009**, *21*, 2055−2061.
(7) Guillemot, F.; Brunet-Bruneau, A.; Bourgeat-Lami, E.; Gacoin, T.; Barthel, E.; Boilot, J.-P. Latex-Templated Silica Films: Tailoring Porosity to Get a Stable Low-Refractive Index. *Chem. Mater.* **2010**, *22*, 2822−2828.
(8) Shimizu, W.; Murakami, Y. Microporous Silica Thin Films with Low Refractive Indices and High Young's Modulus. *ACS Appl. Mater. Interfaces* **2010**, *2*, 3128−3133.
(9) Seino, M.; Wang, W.; Lofgreen, J. E.; Puzzo, D. P.; Manabe, T.; Ozin, G. A. Low-k Periodic Mesoporous Organosilica with Air Walls: POSS-PMO. *J. Am. Chem. Soc.* **2011**, *133*, 18082−18085.
(10) Wicht, G.; Ferrini, R.; Schüttel, S.; Zuppiroli, L. Nanoporous Films with Low Refractive Index for Large-Surface Broad-Band Anti-Reflection Coatings. *Macromol. Mater. Eng.* **2010**, *295*, 628−636.
(11) Cook, K. T.; Tettey, K. E.; Bunch, R. M.; Lee, D.; Nolte, A. J. One-Step Index-Tunable Antireflection Coatings from Aggregated Silica Nanoparticles. *ACS Appl. Mater. Interfaces* **2012**, *4*, 6426−6431.
(12) Rouse, J. H.; Ferguson, G. S. Preparation of Thin Silica Films with Controlled Thickness and Tunable Refractive Index. *J. Am. Chem. Soc.* **2003**, *125*, 15529−15536.
(13) Hoshikawa, Y.; Yabe, H.; Nomura, A.; Yamaki, T.; Shimojima, A.; Okubo, T. Mesoporous Silica Nanoparticles with Remarkable Stability and Dispersibility for Antireflective Coatings. *Chem. Mater.* **2010**, *22*, 12−14.
(14) Moghal, J.; Kobler, J.; Sauer, J.; Best, J.; Gardener, M.; Watt, A. A. R.; Wakefield, G. High-Performance, Single-Layer Antireflective Optical Coatings Comprising Mesoporous Silica Nanoparticles. *ACS Appl. Mater. Interfaces* **2012**, *4*, 854−859.
(15) Xu, L.; He, J. Antifogging and Antireflection Coatings Fabricated by Integrating Solid and Mesoporous Silica Nanoparticles without Any Post-Treatments. *ACS Appl. Mater. Interfaces* **2012**, *4*, 3293−3299.
(16) Kobler, J.; Möller, K.; Bein, T. Colloidal Suspensions of Functionalized Mesoporous Silica Nanoparticles. *ACS Nano* **2008**, *2*, 791−799.
(17) Kobler, J.; Bein, T. Porous Thin Films of Functionalized Mesoporous Silica Nanoparticles. *ACS Nano* **2008**, *2*, 2324−2330.
(18) Zhang, K.; Xu, L.-L.; Jiang, J.-G.; Calin, N.; Lam, K.-F.; Zhang, S.-J.; Wu, H.-H.; Wu, G.-D.; Albela, B.; Bonneviot, L.; Wu, P. Facile Large-Scale Synthesis of Monodisperse Mesoporous Silica Nanospheres with Tunable Pore Structure. *J. Am. Chem. Soc.* **2013**, *135*, 2427−2430.
(19) Gombert, A.; Glaubitt, W.; Rose, K.; Dreibholz, J.; Bläsi, B.; Heinzel, A.; Sporn, D.; Döll, W.; Wittwer, V. Subwavelength-Structured Antireflective Surfaces on Glass. *Thin Solid Films* **1999**, *351*, 73−78.
(20) Wu, F.; Shi, G.; Xu, H.; Liu, L.; Wang, Y.; Qi, D.; Lu, N. Fabrication of Antireflective Compound Eyes by Imprinting. *ACS Appl. Mater. Interfaces* **2013**, *5*, 12799−12803.
(21) Päivänranta, B.; Sahoo, P. K.; Tocce, E.; Auzelyte, V.; Ekinci, Y.; Solak, H. H.; Liu, C.-C.; Stuen, K. O.; Nealey, P. F.; David, C. Nanofabrication of Broad-Band Antireflective Surfaces Using Self-Assembly of Block Copolymers. *ACS Nano* **2011**, *5*, 1860−1864.
(22) Schulz, U.; Munzert, P.; Rickelt, F.; Kaiser, N. Hybrid Antireflective Coating with Plasma-Etched Nanostructure. *Thin Solid Films* **2013**, *532*, 119−122.
(23) Ji, S.; Song, K.; Nguyen, T. B.; Kim, N.; Lim, H. Optimal Moth Eye Nanostructure Array on Transparent Glass Towards Broadband Antireflection. *ACS Appl. Mater. Interfaces* **2013**, *5*, 10731−10737.
(24) Xi, J.-Q.; Schubert, M. F.; Kim, J. K.; Schubert, E. F.; Chen, M.; Lin, S.-Y.; Liu, W.; Smart, J. A. Optical Thin-Film Materials with Low Refractive Index for Broadband Elimination of Fresnel Reflection. *Nat. Photonics* **2007**, *1*, 176−179.
(25) Ravipati, S.; Shieh, J.; Ko, F.-H.; Yu, C.-C.; Chen, H.-L. Ultralow Reflection from *a*-Si Nanograss/Si Nanofrustum Double Layers. *Adv. Mater.* **2013**, *25*, 1724−1728.
(26) Cox, A. J.; DeWeerd, A. J.; Linden, J. An Experiment to Measure Mie and Rayleigh Total Scattering Cross Sections. *Am. J. Phys.* **2002**, *70*, 620−625.
(27) Gabriel, G. J. Microscopic Theory of Rayleigh Scattering. *Phys. Rev. A: At., Mol., Opt. Phys.* **1973**, *8*, 963−990.
(28) Joo, W.; Kim, Y.; Jang, S.; Kim, J. K. Antireflection coating with enhanced anti-scratch property from nanoporous block copolymer template. *Thin Solid Films* **2011**, *519*, 3804−3808.

DOI: 10.1021/acsami.5b05659
ACS Appl. Mater. Interfaces 2015, 7, 19424−19430